CAMBRIDGE
UNIVERSITY PRESS

Article

Investigation of unexplored kaolin occurrences in southern Mauritania and preliminary assessment of possible applications

D. Küster[1], Stephan Kaufhold[1]* , Emanetoullah Limam[2], Omar Jatlaoui[1], Oumar Ba[2],

Abdellahi Maham Zein Mohamed[2], M. Pohlmann-Lortz[3], M. Ranneberg[1] and K. Ufer[1]

[1]BGR, Stilleweg 2, D-30655 Hannover, Germany; [2]Agence Nationale de Recherches Géologiques et du Patrimoine Minier (ANARPAM), Nouakchott, Mauritania and [3]Forschungsinstitut für Anorganische Werkstoffe – Glas/Keramik – GmbH (FGK), Heinrich-Meister-Straße 2, D-56203 Höhr-Grenzhausen, Germany

Abstract

Non-metallic raw materials are largely unexplored in many African countries. In an attempt to reduce this knowledge gap, kaolin occurrences in three promising regions of southern Mauritania were examined. The aim of the paper is to describe the occurrences and characterize the material in terms of mineralogy and potential technical use in the ceramics industry. The kaolins are geologically associated with various sedimentary rock units in either the Coastal Basin (Kaédi), the Mauritanide Belt (Hassi Abyad) or the Taoudeni Basin (Néma). Geochemical data show Al_2O_3 contents of between 9% and 38% (corresponding to 23–96% kaolinite). Samples from the Hassi Abyad and Kaédi regions have greater kaolinite contents on average and were further investigated mineralogically. The kaolin from the Néma region contained less kaolinite (<50 mass%). The region is also less accessible and hence is not considered further in this study. X-ray diffraction, X-ray fluorescence and infrared spectroscopy confirmed the geochemically calculated kaolinite contents of the kaolins and identified quartz, anatase and goethite as the remaining major mineral constituents. The degree of structural disorder of the kaolinites (determined by infrared spectroscopy) is generally greater in the Kaédi occurrences than at Hassi Abyad. Ceramic tests proved that all of these kaolin raw materials might be used for the production of ceramics, and some may even be used for fine ceramics. From an economic point of view, the Hassi Abyad deposit is interesting in terms of its quality and reserves, aspects that will be addressed in detail in a follow-up study.

Kaolin is a valuable industrial clay with a large variety of applications. In its raw form kaolin has limited applications, mainly as a raw material for various types of ceramic products or as a white pigment for decoration and painting. More technically demanding applications (ceramics, functional filler in paper, plastics, amongst others) require thoroughly refined and selectively processed mineral products. Markets for these end-product applications usually exist in industrialized economies, where the added value of the final mineral products is also of major concern.

In less-developed or non-industrialized economies, kaolin mining and processing is limited, primarily due to a lack of substantial local manufacturing industries and respective markets for refined kaolin mineral products. This is the case in Africa. Although >250 kaolin occurrences are known on the continent (Ekosse, 2010), exploitation on a greater scale is restricted to the Republic of South Africa and Egypt. Small-scale operations in countries such as Algeria, Botswana, Ethiopia, Nigeria and Tanzania, among others, are directed mainly at the production of bricks and ceramics (Ekosse, 2010).

Incentives to invest in kaolin exploration, mining and processing in Africa are rather restricted due to the lack of markets for added-value products. The value-adding potential of kaolin extraction and refinement can, however, also be seen as a stimulus for local economic development in less-developed countries (Ekosse, 2010). In such countries, exploration of kaolin occurrences and the evaluation of the mineralogical and technical properties of kaolin raw materials are mainly undertaken by public organizations (i.e. geological surveys), especially during the first stages of exploration. Within this framework, the present study was undertaken during a project on mining-sector diversification in Mauritania, jointly carried out by Bundesanstalt für Geowissenschaften und Rohstoffe (BGR) and Office Mauritanien de Recherches Géologiques (OMRG) (now Agence Nationale de Recherches Géologiques et du Patrimoine Minier (ANARPAM)).

Geological features of kaolin deposits with reference to western Africa

Kaolins may be either of primary (residual, hydrothermal, mixed) or of secondary (sedimentary) origin (Harvey & Murray, 1997). A more detailed classification is provided by Dill (2016). In this paper, however, classification is based on Harvey & Murray (1997) because of insufficient geological data. Primary kaolins form *in situ* through weathering and/or hydrothermal alteration

of feldspathic rocks such as granites and arkoses. Secondary kaolins are derived from the erosion and transport of weathered materials away from their source area, combined with size fractionation during transport and eventual (re)deposition as clastic kaolinite-rich sediments. Some of the most economically important secondary kaolins were further altered after deposition in groundwater environments by microbially mediated processes that naturally removed iron-bearing accessory minerals (Hurst & Pickering, 1997).

In Africa, kaolin outcrops occur in almost every country, with a relatively large number of deposits known to occur in the southern, western and west-central parts of the continent (Ekosse, 2010). Approximately 50% of all kaolin occurrences in Africa are secondary sedimentary and 35% are primary of residual origin. The remaining 15% are classified as mixed or hydrothermal. Known primary kaolin occurrences are located mainly in southern and central Africa (Harvey & Murray, 1997; Murray, 1998; Njoya *et al.*, 2006; Ekosse, 2010). Secondary kaolins occur mostly in northern Africa, but some significant deposits have also been reported in southern and western Africa (Ekosse, 2010). Deposits with a hydrothermal origin are mostly located in central and western Africa (e.g. Njoya *et al.*, 2006; Ekosse, 2010).

Worldwide, most of the sedimentary kaolins occur geologically in Cretaceous and Tertiary strata (Murray, 1998). Among them, the largest and purest kaolins are the fluvial and nearshore marine Coastal Plain deposits in the south-eastern USA and the fluvial and lacustrine deposits in northern Para State, Brazil (Kogel, 2014). The accumulation of Cretaceous and Tertiary sediments and their depositional environments are generally shared between the eastern coast of the Americas and the western coast of Africa. This reflects their similar geological histories during the breakup of the Pangea supercontinent and the opening of the Atlantic Ocean in the Mesozoic. The occurrence of kaolin deposits in western Africa may therefore be temporally and genetically associated with extensive kaolin deposits in the south-eastern USA (Georgia, Alabama) and in Brazil (Ekosse, 2010). This may also serve as a clue for the exploration of presently unknown deposits in West Africa, including Mauritania.

Mauritanian kaolin occurrences and their geological setting

To date, Mauritania has not been reported to have substantial deposits of kaolin. In the compilation of African kaolin deposits by Ekosse (2010), only one occurrence is referred to in Mauritania, namely Akjoujt in west-central Mauritania, possibly of hydrothermal origin. Unpublished reports and notes from the OMRG (now ANARPAM), however, indicate the occurrence of more widespread kaolin outcrops in the southern part of the country, probably related to late Cretaceous and Tertiary episodes of weathering (Pitfield *et al.*, 2004), followed by erosion and deposition in terrestrial to coastal sedimentary basins. None of these kaolin outcrops has ever been studied and evaluated in detail, with the exception of analytical data on a single sample from the Kaédi area (Baudet *et al.*, 1987). Therefore, the aim of this study is to characterize mineralogically and geochemically kaolin outcrops in three regions in southern Mauritania, namely Kaédi, Hassi Abyad and Néma (see Fig. 1), which have not been investigated before. The final aim of this study is to evaluate the possible applications of the various raw materials, which has to be based on in-depth characterization and (ceramic) application tests.

Location and regional geology

Mauritanian geology is characterized by five major tectono-structural units (Fig. 1 & Table 1). The kaolins in the Néma region (south-eastern Mauritania) occur in the Taoudeni Basin, the kaolins of the Hassi Abyad region (south-central Mauritania) occur in the Mauritanide Belt and the kaolins from the Kaédi region (south-western Mauritania) occur in the Coastal Basin (see Fig. 1). More detailed descriptions of the kaolin occurrences are given below.

Kaédi region, Coastal Basin

In south-western Mauritania, kaolins occur west of Kaédi and geologically belong to the Miocene Mbidane Formation (Continental Terminal) of the Coastal Basin (Fig. 2). Six outcrops were sampled at the base or along the flanks of escarpments or small inselbergs, exposing the Mbidane Formation around Bababé, Fondé, Bagodine and Rindiao (see Fig. 2).

The Mbidane Formation is composed of terrestrial to shallow-marine clastic sedimentary deposits that have undergone intense lateritization. Kaolin-rich layers 1–5 m thick occur within sedimentary successions consisting mainly of kaolinitic/kaolinized siltstones and sandstones (Limam *et al.*, 2017). The succession is capped by lateritic iron crust (Fig. 3). The kaolin occurrences and sampling points are easily accessible along the major asphalt road linking the regional centre of Kaédi with the capital Nouakchott (Fig. 2).

Hassi Abyad, Mauritanide Belt

In the central part of southern Mauritania, kaolins occur at Hassi Abyad, ~50 km east of the district capital M'Bout. The kaolin at Hassi Abyad crops out in an alluvial plain that dips slightly to the south, following the direction of the main surface-water drainage system (Fig. 4). The kaolin is usually unstratified and rather compact and is exposed on the surface over several square kilometres. It is made up of white kaolinitic clay with reddish, violet and yellow patches (Fig. 5) (Limam *et al.*, 2017). The latter probably originated from (presumably later) infiltrations of weathering solutions.

The kaolin probably overlies altered metasedimentary and metavolcanic schistose rocks of the Mauritanide Belt, which also crop out along the slopes and the upper reaches of the alluvial drainage. However, the direct contact between the kaolin and the Mauritanide Belt rocks is not exposed and their relationship remains unclear. Erosional remnants of a palaeoregolith with complete *in situ* lateritic weathering profiles are exposed in the near surroundings (Fig. 4). The palaeoregolith is considered of Miocene age (Pitfield *et al.*, 2004) and might have derived from the weathering of underlying Mauritanide Belt rocks. The kaolin in the Hassi Abyad plain is, in places, also capped by lateritic iron crust, and it is incised and partly overlain by a thin veneer of fluvial silts and sands, indicating that the kaolin is not a product of recent alluvial deposition. A residual or near-residual formation of the Hassi Abyad kaolin may be suggested.

Initially, a set of four surface samples was taken, which was later supplemented by 35 samples from shallow drillings (Fig. 4). Drilling was conducted due to the apparently huge size of the Hassi Abyad kaolin deposit. Further results from subsequent drillings will be reported in a follow-up paper. The Hassi Abyad deposit is reasonably accessiblevia an earthen road which links Mbout with Kiffa (see Fig. 4).
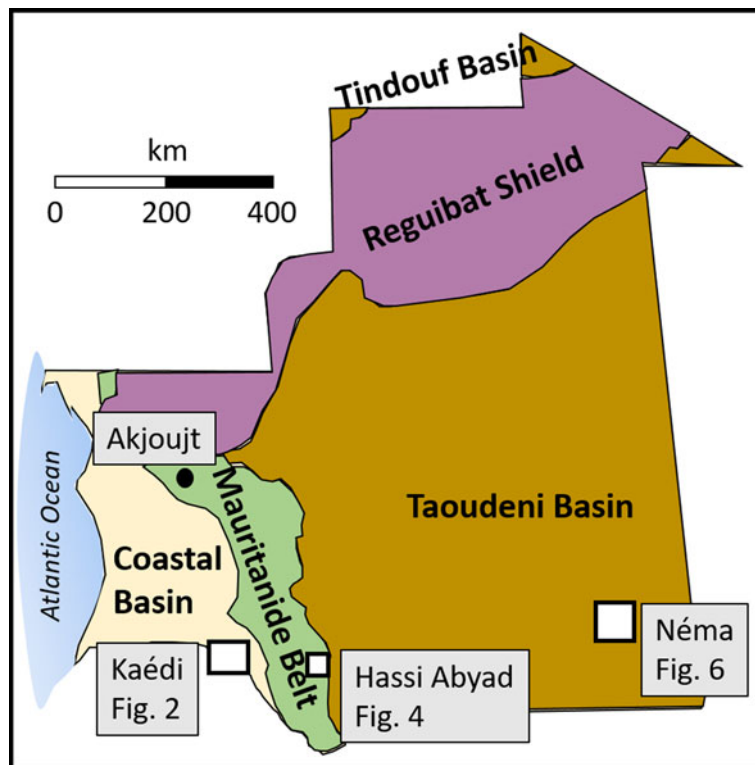
Fig. 1. General geological map of Mauritania indicating the locations of the kaolin occurrences investigated (Kaédi, Hassi Abyad and Néma regions) and of another known kaolin deposit (Akjoujt). The latter was not studied in this paper. Map modified after Langer & Horton (2012).

Table 1. Geological units of Mauritania (OMRG, 2015).

Name of tectono-structural unit	Age and rock associations
Reguibat Shield (Bouclier Réguibat)	Archaean to Palaeoproterozoic magmatic and high-grade metamorphic rocks, part of the West African Craton
Taoudeni Basin (Bassin de Taoudeni)	Neoproterozoic to Palaeozoic sedimentary rocks (outcropping in the west) and Mesozoic to Cenozoic sedimentary rocks (outcropping in the east), forming the sedimentary cover of the West African Craton
Tindouf Basin (Bassin de Tindouf)	Neoproterozoic to Mesozoic sedimentary rocks, to the north of the Reguibat Shield; equivalent in structure and position to the Taoudeni Basin
Mauritanide Belt (Ceinture des Mauritanides)	Neoproterozoic to Palaeozoic magmatic and low-grade metamorphic rocks of volcanosedimentary origin, partly thrusted onto the West African Craton
Coastal Basin (Bassin Côtier)	Mesozoic to Cenozoic sedimentary rocks, formed during the opening of the Atlantic Ocean, overlying Mauritanide Belt rocks

Néma region, Taoudeni Basin

In south-eastern Mauritania, kaolins occur 30–60 km north of Néma and belong geologically to the Lower Cretaceous Néma Group (Continental Intercalaire) of the Taoudeni Basin (Fig. 6). Three kaolin occurrences were sampled between Néma and Oualata, two of which occur along the flanks of an escarpment (samples WA 1 and WA 8; see also Fig. 7), while the third one resides on top of the escarpment and occupies an area >1 km^2 (Limam *et al.*, 2018).

The Néma Group consists of clastic sedimentary rocks, mainly sandstones, discordantly overlying Neoproterozoic to Cambrian

marine shales and siltstones (Fig. 6). The kaolin occurs in the form of lenticular bodies within variably altered and kaolinized sandstones of the Néma Group. The profile is partly capped by a thin ferricrust and is often underlain by pre-Cretaceous partly altered doleritic intrusions (see Fig. 7). Based on these observations, the formation of the kaolin by weathering and alteration of the clastic sedimentary rocks is likely; detailed investigations of the genesis of these occurrences have not been undertaken, however.

The kaolins of the Néma-Oualata region are rather difficult to access and can be reached from Néma, the regional centre, only *via* logistically challenging desert tracks.

Materials and methods

A total of 53 samples were collected from the three regions and were analysed using X-ray fluorescence (XRF). The samples were dried at 60°C for 3 days and ground using a mortar mill prior to analyses. The samples and analyses performed and discussed in the present study are summarized in Table 2.

Samples were ground and mixed with a lithium metaborate flux (Spectroflux, Flux No. 100A, Alfa Aesar) and fused to make glass beads. The beads were analysed using wavelength-dispersive XRF spectroscopy with a PANalytical Axios spectrometer (ALMELO, The Netherlands). To determine loss on ignition (LOI), 1000 mg of sample material was heated at 1030°C for 10 min. A total of 150 reference samples provided by various geological surveys were used for calibration. The materials covered common rocks, soils and ores. Validation of the calibration was performed using mixtures of synthetic oxides. Matrix correction was carried out as described by de Jongh (1973).

The mineralogical composition of the samples was determined using X-ray diffraction (XRD) with a PANalytical X'Pert PRO
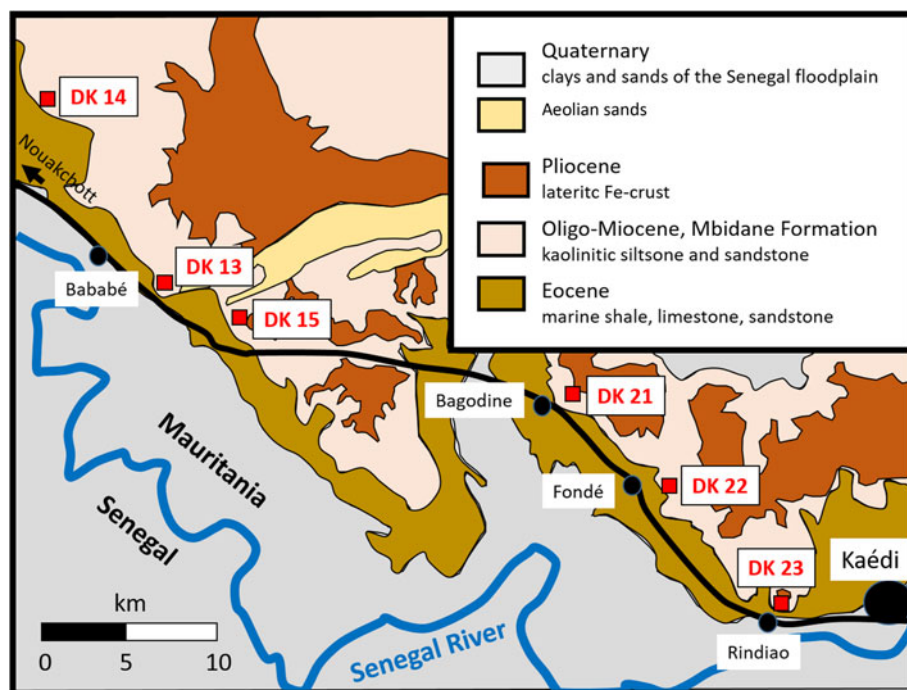
Fig. 2. Geological sketch map showing the locations of the kaolin samples to the west of Kaédi.

Fig. 3. Photographs of kaolin cropping out in the Kaédi region. Kaolinitic layers of the Mbidane Formation, capped by lateritic crust.

MPD θ-θ diffractometer (Co-*K*α radiation, 40 kV and 40 mA), equipped with a variable-divergence slit (20 mm irradiated length), primary and secondary soller slits, diffracted beam monochromator, point detector and sample changer (sample diameter 28 mm). The samples were investigated from 1° to 80°2θ with a step size of 0.03°2θ and a measuring time of 10 s per step. For specimen preparation, the back-loading technique was used. Prior to XRD measurements, the samples were also ground using a McCrone mill.

Rietveld refinement of the experimental XRD data was conducted using the *Profex/BGMN* software (Bergmann *et al.*, 1998; Döbelin & Kleeberg, 2015). The mineral phases were identified during the Rietveld refinement process. No other clay mineral was identified; therefore, the refinements started at 10°2θ. The presence of abundant illite was rejected based on the low K_2O content of the samples. The kaolinite content was derived from Rietveld refinement using two types of kaolinites with various degrees of disorder. The kaolinite content represents the sum of both types (Ufer *et al.*, 2015). Kaolinite contents were also calculated based on the Al_2O_3 content assuming the absence of other Al-bearing minerals and considering that 1mass% kaolinite contains 0.395 mass% Al_2O_3.

Fourier-transform infrared (FTIR) spectra were collected in the mid-infrared (MIR) region using the KBr pellet technique (1 mg sample per 200 mg KBr). Spectra were collected on a Thermo Nicolet Nexus (Nicolet Instruments, USA) FTIR spectrometer (MIR beam splitter: KBr, deuterated triglycine sulfate detector), with a resolution of 2 cm^{-1}. Measurements were conducted before and after drying of the pellets at 150°C in a vacuum oven for 24 h.

The cation-exchange capacity (CEC) of the samples was measured using the Cu-triethylenetetramine (Cu-Trien) method (Meier & Kahr, 1999). Using this method, 10 mL Cu-Trien solutions and 50 mL of deionized water were added to the sample (400 and 600 mg). The mixture was shaken end-over-end for 1 h and subsequently was centrifuged. The amount of Cu-Trien adsorbed was measured with a visible-light spectrometer adjusted to 578 nm.
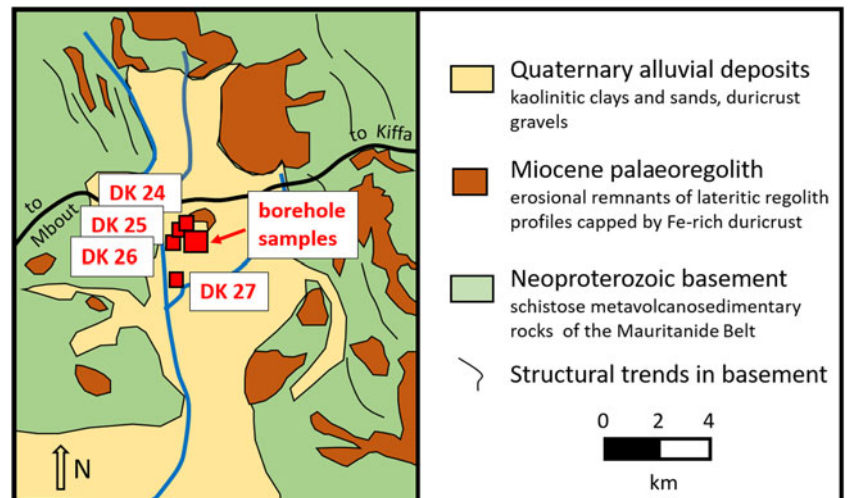
Fig. 4. Geological sketch map showing the locations of the kaolin samples at Hassi Abyad.

Fig. 5. Photographs of kaolin cropping out at Hassi Abyad.
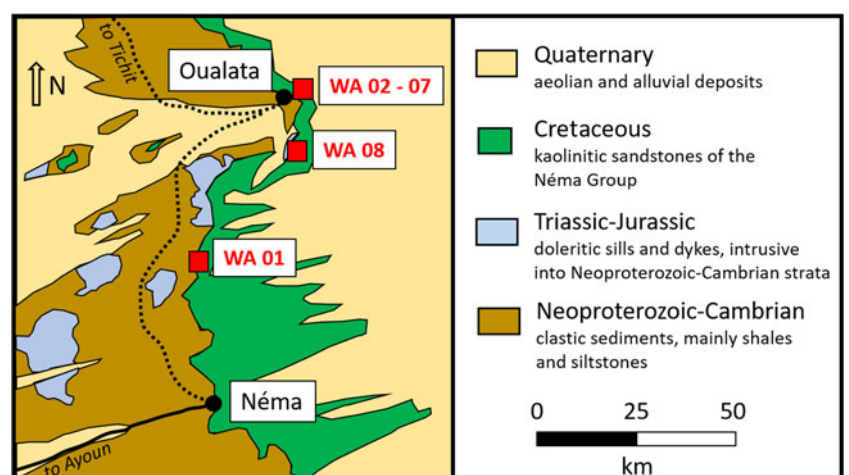
Fig. 6. Geological sketch map showing the locations of the kaolin samples from the Néma region.

The specific surface area of the samples was determined by N_2 adsorption. Measurements were performed using a Micromeritics Gemini III 2375 surface area analyser with samples of ~300 mg in weight. Samples were degassed for 24 h at 105°C under vacuum. Nitrogen adsorption at five different relative pressure values was assessed and the data were used to calculate the Brunauer–Emmett–Teller (BET) surface area.

The organic carbon (C_{org}) content was measured using a LECO CS-444 Analysator (LECO, USA) after dissolution of the carbonates. Carbonates were removed by treating the samples
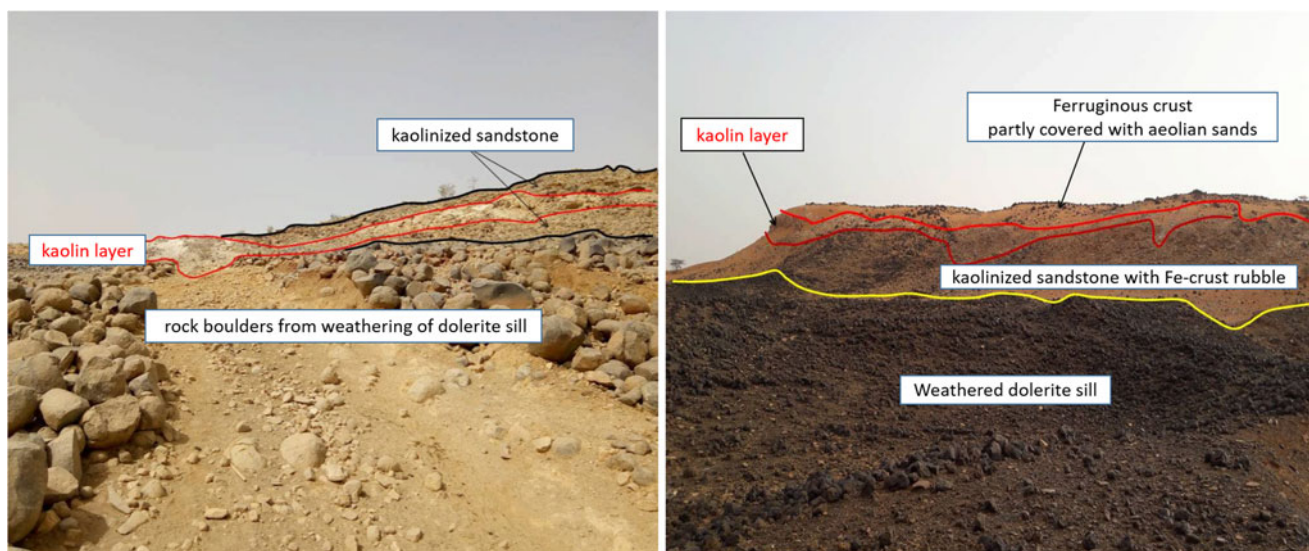
Fig. 7. Photographs of kaolin cropping out in the Néma region. Sub-horizontal, lenticular to irregular kaolin bodies within kaolinized sandstones, underlain by dolerite intrusions.

several times at 80°C with HCl until no further gas evolution could be observed. Samples of 170–180 mg of the dried material were used to measure the total carbon (C_{total}) content. Total inorganic carbon (C_{carb}) was calculated from the difference of C_{total} and C_{org}. The samples were heated in the device to 1800–2000°C in an oxygen atmosphere and the CO_2 and SO_2 were detected using an infrared detector.

Ceramic tests were performed at the FGK, which runs/operates a commercial testing laboratory specialized in testing inorganic materials made of ceramics and glass. The melting behaviour was tested according to DIN 51730 (2007). In addition, the firing shrinkage and colour after firing were determined. Furthermore, the water absorption with open porosity and the tensile strength were determined according to DIN EN 993-1 (2019). Prior to ceramic testing, the samples were dried at 110°C, milled by a jaw crusher and ground by a vibratory disc mill (split width 1 mm). For the production of pressed pieces (pellets), ~6 mass% water was added to each sample. For each sample, 30 pellets with a diameter of 40 mm were produced using a 32 MPa uniaxial load. The mass of each pellet was 20 g. After compaction, the samples were again dried at 110°C and then calcined at various temperatures (1000°C, 1100°C, 1200°C, 1300°C), with a temperature ramp of 5 K min^{-1} and a 30 min soaking time at maximum temperature.

A Zeiss Sigma 300 VP field emission gun scanning electron microscope (SEM) operating at 15 kV was used to evaluate the samples at the micro-scale using the high-vacuum mode. Carbon coating was used to provide sufficient electrical conductivity. The microscope was equipped with the following detectors: a Bruker Xflash® 6/60 energy-dispersive X-ray detector, a high-definition backscattered electron detector (HDBSD), a secondary electron detector (SE2), a variable-pressure secondary electron detector (VPSE) and an InLens detector for the detection of secondary and backscattered electrons, respectively.

Grain-size analysis was performed using X-ray granulometry (XRG) with a SediGraph 5100™ and MasterTech 052 Autosampler™ (Micrometrics, USA). The device is used to measure gravity-induced settling rates of different-sized particles through X-ray absorption of particles in a suspension. Prior to this measurement, the samples were dispersed in a 0.01 N $Na_2P_2O_7 \times 10$ H_2O solution, and the >63 µm fraction was subjected to drying and conventional sieving. The material passing through the 63 µm sieve was freeze-dried and resuspended to fit the requirements of XRG regarding the solution:solid ratio. This procedure also included ultrasonic treatment of the suspension (2 × 2 min at 20 kHz) in addition to a weak ultrasonic short shake-up immediately prior to XRG measurement.

Results and discussion

Chemical composition

Kaolin raw materials are commonly assessed based on their Al_2O_3 content, which is often highly correlated with the kaolinite content (e.g. Dewi *et al.*, 2018). The geochemical data including C and S values of all samples considered in the present study are given in Table 3. Reference chemical compositions for commercial kaolins were published by Harben (1992).

The Al_2O_3 content of the samples from the Kaédi region ranged from ~10 to 31 mass%, corresponding to a kaolinite content ranging from 25 to 80 mass%. The Fe_2O_3 content of the kaolinite-rich materials was small (<2 mass%), as was the inorganic carbon content. The C contents ranged from 0.1 to 0.3 mass% and could be largely explained by the presence of organic C rather than carbonates. The carbonate content hence is low, which is favourable for some ceramic applications. Relatively high P contents (0.1–1.0 mass%) as well as Sr contents (up to 3000 mg kg^{-1}) were identified. Samples from Hassi Abyad, by contrast, had greater TiO_2 contents (>1 mass%), maximum Sr contents of ~1000 mg kg^{-1} and a very small organic carbon content on average. The Al_2O_3 content of the Hassi Abyad samples indicated the presence of up to 96 mass% kaolinite and >80 mass% kaolinite on average. The kaolins from the Kaédi and Hassi Abyad regions have variable Fe_2O_3 contents, but the kaolins from the Néma region are more homogeneous with respect to Fe_2O_3 content. The geochemical variation of the samples from the Néma region was comparably low, but the kaolinite contents did not exceed 50 mass% (based on the Al_2O_3 values of 17–18 mass%). In addition, the region is not easily accessible.

Table 2. Samples collected from the three kaolin-bearing regions and the analytical methods used in the present study.

	Deposit	XRF	LECO C/S values	XRD Rietveld	IR spectroscopy	Ceramic tests	CEC	N_2-BET	SEM	PSD
DK13	Kaédi	√	√	√	√	√	√	√		√
DK14	Kaédi	√	√	√	√	√	√	√		√
DK15	Kaédi	√	√	√	√	√	√	√		√
DK21	Kaédi	√	√	√	√	√	√	√	√	√
DK22	Kaédi	√	√	√	√	√	√	√	√	√
DK23	Kaédi	√	√	√	√	√	√	√		√
DK24	Hassi Abyad	√	√	√	√	√	√	√		√
DK25	Hassi Abyad	√	√	√	√	√	√	√	√	√
DK26	Hassi Abyad	√	√	√	√	√	√	√		√
DK27	Hassi Abyad	√	√	√	√	√	√	√	√	√
DK183	Hassi Abyad	√	√							
DK190	Hassi Abyad	√	√							
DK196	Hassi Abyad	√	√							
DK198	Hassi Abyad	√	√							
DK214	Hassi Abyad	√	√							
DK221	Hassi Abyad	√	√							
DK230	Hassi Abyad	√	√							
DK237	Hassi Abyad	√	√							
DK238	Hassi Abyad	√	√							
DK239	Hassi Abyad	√	√							
DK250	Hassi Abyad	√	√							
DK252	Hassi Abyad	√	√							
DK293	Hassi Abyad	√	√							
DK294	Hassi Abyad	√	√							
DK300	Hassi Abyad	√	√							
DK301	Hassi Abyad	√	√							
DK303	Hassi Abyad	√	√							
DK308	Hassi Abyad	√	√							
DK309	Hassi Abyad	√	√							
DK310	Hassi Abyad	√	√							
DK311	Hassi Abyad	√	√							
DK313	Hassi Abyad	√	√							
DK314	Hassi Abyad	√	√							
DK317	Hassi Abyad	√	√							
DK322	Hassi Abyad	√	√							
DK383	Hassi Abyad	√	√							
DK393	Hassi Abyad	√	√							
DK394	Hassi Abyad	√	√							
DK395	Hassi Abyad	√	√							
DK398	Hassi Abyad	√	√							
DK399	Hassi Abyad	√	√							
DK407	Hassi Abyad	√	√							
DK412	Hassi Abyad	√	√							
DK413	Hassi Abyad	√	√							
DK415	Hassi Abyad	√	√							
wa 001	Néma	√	√							
wa 002	Néma	√	√							
wa 003	Néma	√	√							
wa 004	Néma	√	√							
wa 005	Néma	√	√							
wa 006	Néma	√	√							
wa 007	Néma	√	√							
wa 008	Néma	√	√							

PSD = particle-size distribution.

Therefore, the study focused on the kaolins from the Kaédi and Hassi Abyad deposits. The trace element composition showed relatively large Cr contents, suggesting at least andesitic parent rocks and comparably high Sr contents. The most significant Sr contents are marked in italics in Table 3.

Mineralogical characterization

A summary of the mineralogical composition of selected samples from the Kaédi and Hassi Abyad deposits is given in Table 4.

The CEC values of all samples from both deposits are small, indicating traces or the absence of swelling clay minerals. A CEC value of 2 or 3 meq 100 g^{-1} is attributed to the variable charge of the kaolinites (Kaufhold & Dohrmann, 2013). The BET specific surface area is commonly controlled by micropores, but in the case of kaolinites, which do not possess micropores, it is controlled by the particle size. Well-crystallized kaolinites have specific surface areas of <10 m^2 g^{-1}. The specific surface areas of samples from both deposits considered in the present study, by contrast, was ~20 m^2 g^{-1}, pointing towards the presence of small kaolinite particles. Specific surface areas of <20 m^2 g^{-1} were observed in the samples with the smallest kaolinite contents (e.g. sample DK22, with a specific surface area of 6 m^2 g^{-1}, contains 24% kaolinite).

Table 3. Geochemical data of all samples. Al$_2$O$_3$ contents are often used as kaolin quality indicators and hence are marked in bold. Values marked with italics are significant.

		SiO$_2$	TiO$_2$	Al$_2$O$_3$	Fe$_2$O$_3$	MnO	MgO	CaO	Na$_2$O	K$_2$O	P$_2$O$_5$	(SO$_3$)	LOI	Sum	Ba	Ce	Co	Cr	Cu	Ga	La	Nb	Nd	Ni	Pb	Sc	Sr	Th	V	Y	Zn	Zr	C$_{tot}$	C$_{org}$	C$_{carb}$	S$_{tot}$
		(mass%)/(mg kg^{-1})																																		
DK13	Kaédi	55	0.9	**31**	1.0	0.0	0.1	0.1	0.0	0.1	0.2	0.0	12	99.8	125	154	<6	167	18	23	65	18	81	15	21	<23	427	15	49	20	15	151	0.3	0.3	0.0	0.0
DK14		59	1.0	**26**	1.6	0.0	0.2	0.2	0.1	0.1	0.6	0.0	11	99.5	266	217	<6	161	16	26	82	20	182	17	25	<23	*2409*	18	75	39	17	272	0.2	0.1	0.0	0.1
DK15		59	1.0	**25**	1.2	0.0	0.1	0.5	0.2	0.1	1.0	0.1	11	99.4	405	127	<6	158	19	22	45	21	141	11	23	<23	*3149*	18	70	69	11	269	0.2	0.1	0.0	0.1
DK21		72	0.3	**18**	1.5	0.0	0.1	0.1	0.1	0.1	0.3	0.0	7	99.8	211	160	<6	128	18	10	54	8	133	17	9	<23	702	18	86	19	9	270	0.3	0.2	0.0	0.0
DK22		83	0.8	**9**	0.4	0.0	0.1	0.4	0.1	0.0	0.1	0.0	5	99.8	76	67	<6	68	18	13	49	18	<36	6	13	<23	238	16	24	20	11	523	0.2	0.2	0.0	0.0
DK23		58	0.9	**19**	12.4	0.0	0.1	0.1	<0.01	0.0	0.3	0.0	9	99.7	165	93	<9	200	20	18	42	15	92	26	23	<24	522	22	129	28	78	603	0.3	0.2	0.0	0.0
DK24	Hassi Abyad	43	1.2	**36**	1.6	0.0	0.2	2.0	0.1	0.0	0.1	0.1	16	99.7	236	159	<6	192	97	51	92	26	51	34	71	35	320	28	138	28	28	267	0.7	0.2	0.5	0.0
DK25		44	1.7	**38**	1.0	0.0	0.1	0.1	0.0	0.0	0.1	<0.01	15	99.8	206	151	<6	198	101	59	76	34	58	37	65	23	368	24	79	31	21	290	0.2	0.1	0.0	0.0
DK26		44	2.0	**37**	1.4	0.0	0.1	0.1	0.0	0.0	0.1	0.0	15	99.7	355	142	<6	197	89	57	74	41	58	35	56	25	526	25	147	28	20	347	0.2	0.1	0.0	0.0
DK27		47	2.6	**35**	1.0	0.0	0.2	0.1	0.1	0.0	0.1	<0.01	14	99.8	82	148	<6	204	27	51	78	55	<35	46	56	27	77	29	75	32	21	631	0.2	0.2	0.0	0.0
DK183		46	2.0	**35**	1.7	0.0	0.1	0.1	0.0	0.0	0.2	0.0	14	99.7	383	187	<6	177	78	50	72	45	81	25	39	27	531	29	131	31	22	486	0.1	0.1	0.0	0.1
DK190		45	1.6	**36**	2.1	0.0	0.1	0.0	0.0	0.0	0.1	0.0	14	99.7	177	120	<6	193	97	57	67	33	58	35	40	37	306	22	133	31	22	288	0.0	0.0	0.0	0.1
DK196		48	2.0	**34**	1.6	0.0	0.1	0.1	0.1	0.1	0.2	0.0	14	99.7	434	158	<6	171	73	51	84	45	78	26	39	30	585	30	114	54	22	503	0.0	0.0	0.0	0.0
DK198		44	2.0	**36**	1.8	0.0	0.1	0.1	0.1	0.1	0.2	0.0	15	99.6	590	150	<6	193	76	52	75	41	53	35	41	46	914	27	169	53	21	360	0.0	0.0	0.0	0.1
DK214		44	1.7	**36**	2.1	0.0	0.1	0.1	0.0	0.0	0.2	0.0	15	99.7	474	151	<6	185	54	51	63	36	81	29	40	24	794	25	160	30	20	332	0.1	0.1	0.0	0.1
DK221		51	1.7	**27**	8.4	0.0	0.1	0.0	0.0	0.1	0.2	0.0	11	99.7	331	144	<8	208	75	36	59	39	70	24	33	29	476	25	281	29	28	540	0.1	0.1	0.0	0.0
DK230		45	2.6	**34**	3.7	0.0	0.1	0.1	0.0	0.0	0.1	0.0	14	99.7	252	169	<7	225	66	55	67	53	61	35	38	26	372	23	157	32	19	534	0.0	0.0	0.0	0.0
DK237		48	1.9	**25**	12.0	0.0	0.1	0.1	0.0	0.1	0.2	0.0	12	99.6	382	112	<9	276	59	36	75	39	62	25	30	25	487	22	396	31	22	536	0.2	0.2	0.0	0.0
DK238		46	2.1	**33**	4.7	0.0	0.1	0.0	0.1	0.1	0.2	0.0	14	99.6	636	150	<7	203	68	45	80	43	78	31	34	29	881	25	229	30	23	438	0.1	0.1	0.0	0.1
DK239		45	2.2	**35**	2.6	0.0	0.1	0.0	0.1	0.1	0.3	0.0	14	99.5	856	120	<6	216	80	51	65	43	85	32	36	25	*1290*	25	182	32	20	389	0.1	0.1	0.0	0.1
DK250		50	1.8	**32**	2.4	0.0	0.1	0.1	0.0	0.1	0.2	<0.01	13	99.7	397	169	<6	178	55	39	68	40	87	26	33	<23	529	27	138	31	27	525	0.1	0.1	0.0	0.0
DK252		55	1.8	**28**	2.6	0.0	0.1	0.1	0.0	0.1	0.2	0.02	12	99.6	611	180	<6	157	55	39	77	38	98	24	35	25	948	27	163	36	22	474	0.1	0.1	0.0	0.1
DK293		48	1.7	**30**	6.2	0.0	0.2	0.2	0.0	0.1	0.2	0.01	13	99.7	394	127	<7	210	71	43	61	35	66	34	35	31	515	25	192	31	31	458	0.1	0.1	0.0	0.0
DK294		48	1.7	**34**	2.3	0.0	0.1	0.1	0.0	0.1	0.1	0.02	14	99.7	310	149	<6	201	70	51	78	35	50	41	39	<23	454	25	96	30	26	383	0.1	0.1	0.0	0.0
DK300		51	1.4	**24**	12	0.0	0.2	0.1	0.1	0.2	0.2	0.02	11	99.7	290	122	<9	220	52	34	49	32	53	31	28	<23	325	22	323	28	17	495	0.1	0.1	0.0	0.0
DK301		49	1.6	**29**	6.1	0.0	0.2	0.1	0.1	0.2	0.1	0.01	13	99.7	324	141	<7	196	57	42	80	36	74	28	36	31	452	30	202	33	20	465	0.1	0.1	0.0	0.0
DK303		49	1.6	**30**	5.2	0.0	0.1	0.1	0.0	0.1	0.1	0.02	13	99.7	342	146	<7	229	53	41	72	34	65	28	32	<23	483	24	174	28	27	452	0.1	0.1	0.0	0.0
DK308		53	1.9	**29**	2.7	0.0	0.1	0.1	0.1	0.1	0.2	0.01	12	99.6	506	182	<6	169	34	39	82	38	104	23	32	<23	657	30	149	31	27	537	0.2	0.2	0.0	0.0
DK309		50	1.8	**32**	2.5	0.0	0.2	0.1	0.0	0.1	0.2	0.01	13	99.6	452	173	<6	190	42	42	82	40	92	26	33	32	589	25	159	36	24	528	0.1	0.1	0.0	0.0
DK310		53	1.9	**31**	1.9	0.0	0.1	0.1	0.0	0.1	0.2	0.01	12	99.7	404	184	<6	176	44	37	73	41	92	23	38	29	551	26	118	31	22	492	0.1	0.1	0.0	0.0
DK311		56	1.8	**28**	1.7	0.0	0.1	0.1	0.0	0	0.2	0.02	11	99.7	450	175	<6	147	45	38	90	40	99	23	33	32	647	24	124	30	18	419	0.0	0.0	0.0	0.0
DK313		46	1.9	**35**	1.8	0.0	0.1	0.1	0.1	0.1	0.2	0.01	14	99.7	474	161	<6	175	35	48	78	43	103	26	36	54	668	28	167	36	20	480	0.0	0.0	0.0	0.1
DK314		45	1.9	**36**	1.4	0.0	0.1	0.1	0.0	0.1	0.2	0.02	15	99.6	570	174	<6	174	46	48	78	41	99	27	34	42	806	27	142	35	24	395	0.0	0.0	0.0	0.1
DK317		44	2.1	**37**	1.3	0.0	0.1	0.1	0.1	0.1	0.2	0.02	15	99.6	567	165	<6	205	38	57	74	43	75	35	43	37	935	24	209	39	22	403	0.0	0.0	0.0	0.2
DK322		46	2	**34**	3.3	0.0	0.1	0.1	0.0	0.1	0.2	0.01	14	99.7	392	174	<6	183	66	49	79	45	81	28	32	27	597	27	179	35	21	524	0.1	0.1	0.0	0.0
DK383		48	1.6	**32**	3.4	0.0	0.2	0.1	0.1	0.1	0.1	0.01	14	99.7	403	157	<6	165	67	45	70	34	78	33	33	35	490	25	159	61	26	399	0.1	0.1	0.0	0.0
DK393		53	2.1	**31**	1.3	0.0	0.1	0.1	0.0	0.1	0.2	0.02	12	99.6	502	161	<6	173	176	42	79	48	75	27	36	57	753	25	81	39	30	563	0.0	0.0	0.0	0.1
DK394		49	2.2	**33**	2.1	0.0	0.1	0.1	0.0	0.1	0.3	0.02	13	99.5	701	188	<6	176	151	46	86	46	121	27	39	31	*1219*	24	147	50	33	511	0.1	0.1	0.0	0.1
DK395		47	2.1	**35**	1.7	0.0	0.1	0.1	0.0	0.1	0.2	0.01	14	99.7	382	159	<6	170	100	48	75	47	83	26	38	30	592	29	117	41	30	515	0.0	0.0	0.0	0.0
DK398		45	1.7	**35**	1.9	0.0	0.1	0.1	0.1	0.1	0.2	0.02	15	99.6	533	144	<6	176	52	52	74	38	58	33	38	28	849	25	258	63	29	357	0.1	0.1	0.0	0.2
DK399		46	1.9	**35**	1.4	0.0	0.1	0.1	0.1	0.1	0.2	0.02	15	99.6	472	158	<6	195	54	57	81	40	75	33	41	24	933	24	186	77	24	415	0.0	0.0	0.0	0.2
DK407		47	1.7	**34**	2.7	0.0	0.2	0.1	0.1	0.1	0.2	0.02	14	99.7	357	149	<6	171	62	48	83	39	64	28	36	27	480	29	128	61	24	431	0.0	0.0	0.0	0.1
DK412		51	1.5	**26**	8	0.0	0.2	0.1	0.0	0.2	0.1	<0.01	12	99.7	243	133	<8	204	52	39	73	35	78	28	31	31	323	25	234	26	20	480	0.2	0.2	0.0	0.0
DK413		50	1.7	**28**	7.4	0.0	0.1	0.1	0.0	0.1	0.2	0.01	12	99.6	390	173	<8	205	57	39	66	38	88	31	33	<23	564	24	224	35	22	504	0.1	0.1	0.0	0.0
DK415		46	2	**34**	3	0.0	0.1	0.1	0.0	0.1	0.2	0.01	14	99.5	355	160	<6	176	62	48	70	46	96	31	38	<23	500	28	155	33	20	517	0.1	0.1	0.0	0.0
wa 001	Néma	72	0.7	**18**	0.7	0.0	0.2	0.1	0.0	0.5	0.4	<0.01	7	99.6	*1421*	474	<5	122	42	24	245	11	225	6	23	<23	572	9	82	32	16	186	n.d.	n.d.	n.d.	n.d.
wa 002		72	0.7	**17**	3.3	0.1	0.1	<0.01	0.1	0.1	0	7	99.9	<63	82	<7	93	81	22	<40	12	54	11	7	25	18	11	184	107	14	167	n.d.	n.d.	n.d.	n.d.
wa 003		72	0.7	**18**	1.5	0.0	0.2	0.2	0.0	0.4	0.1	<0.01	7	99.9	142	<53	<6	100	54	25	<40	12	40	9	15	<24	36	9	92	80	8	164	n.d.	n.d.	n.d.	n.d.
wa 004		71	0.7	**17**	3.5	0.0	0.2	0.3	0.0	0.3	0.1	<0.01	7	99.9	242	64	<7	98	68	23	<40	10	<36	24	13	25	147	11	133	48	22	170	n.d.	n.d.	n.d.	n.d.
wa 005		72	0.6	**17**	1.8	0.0	0.2	0.3	0.1	0.3	0.1	<0.01	7	99.9	242	88	<6	90	44	19	<39	10	90	9	8	<23	219	10	94	122	14	153	n.d.	n.d.	n.d.	n.d.
wa 006		72	0.6	**17**	2.7	0.0	0.1	0.1	0.0	0.2	0.3	<0.01	7	99.7	504	173	<6	62	69	22	59	17	170	10	32	25	423	13	153	146	16	167	n.d.	n.d.	n.d.	n.d.
wa 007		72	0.5	**17**	2.4	0.0	0.1	0.1	<0.01	0.2	0.3	<0.01	7	99.7	576	334	<6	64	57	21	102	19	379	10	19	<23	583	14	110	140	9	163	n.d.	n.d.	n.d.	n.d.
wa 008		73	0.7	**18**	1.1	0.0	0.1	0.1	<0.01	0.1	0.1	<0.01	7	99.8	288	103	<6	125	97	24	40	11	148	16	14	<23	235	12	94	25	14	190	n.d.	n.d.	n.d.	n.d.

Table 4. Mineralogical composition of selected samples from Kaédi and Hassi Abyad. Contents <1 mass% are declared as '0'. The most significant parameter (kaolinite content) is marked in bold.

		DK13 Kaédi	DK14 Kaédi	DK15 Kaédi	DK21 Kaédi	DK22 Kaédi	DK23 Kaédi	DK24 Hassi Abyad	DK25 Hassi Abyad	DK26 Hassi Abyad	DK27 Hassi Abyad
CEC (meq 100 g^{-1})		3	3	2	1	1	1	3	3	2	2
BET (m^2 g^{-1})		18	21	15	9	6	12	22	23	23	20
Kaolinite modal	≤(mass%)	**78**	**65**	**64**	**46**	**24**	**47**	**90**	**96**	**95**	**89**
39.5 mass% Al$_2$O$_3$ for pure kaolinite											
Rietveld analysis											
Kaolinite		**81**	**69**	**66**	**49**	**24**	**49**	**92**	**97**	**97**	**91**
Quartz		17	27	30	49	75	35	1	0	0	5
Crandallite		1	1		0						
Svanbergite		0	2	3	1		1	0	1	1	0
Halite				0		0					
Goethite							14				
Anatase		1	1	0	0	0	1	1	2	2	3
Calcite								5			
Hematite								0			
Pyrite								0			
Rutile		1	0	0		0	1	0	0	0	1
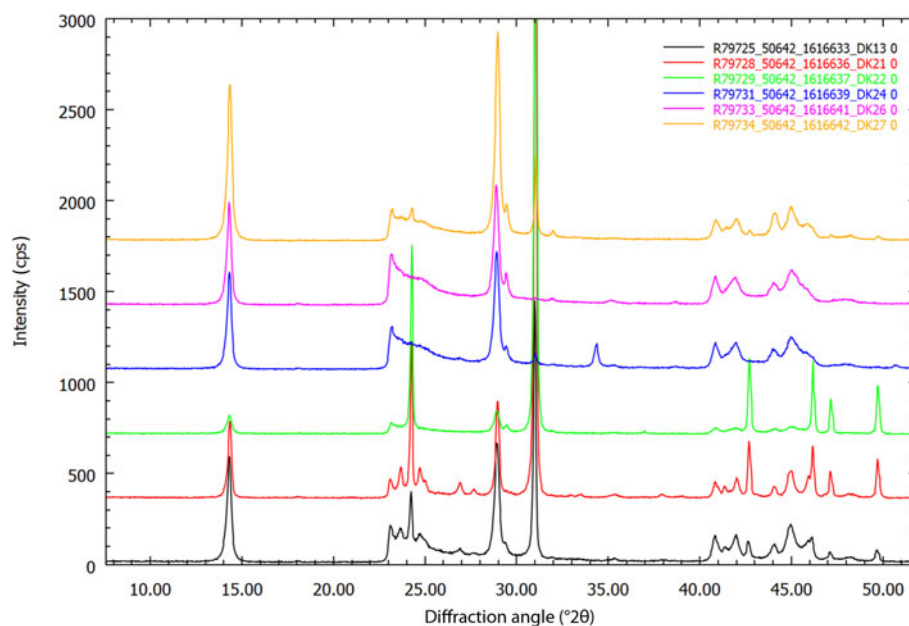
Fig. 8. XRD powder traces of six samples from both promising deposits (uppermost pattern: Hassi Abyad; lowermost pattern: Kaédi).

Two methods were used to determine the kaolinite content: XRF and Rietveld analysis with XRD. Assuming that an Al$_2$O$_3$ content of pure kaolinite accounts for 39.5 mass% and that other Al-bearing minerals are absent, the modal kaolinite content can be calculated based on the Al$_2$O$_3$ content. This method is used routinely in the clay industry. The kaolinite contents obtained from these two methods are in quite good agreement. Using XRD, two different phosphate minerals were distinguished: Ca- and Sr-dominated (crandallite and svanbergite). A reasonable correlation was found between the svanbergite content and the Sr content, which indicates that both related P compounds could be distinguished well by XRD. Apart from crandallite and svanbergite, there is a variety of so-called 'aluminium phosphates and sulfates' minerals (Dill, 2001), which are barely detectable in many clays, though they may be present in minor amounts. Therefore, the identification of svanbergite by XRD in the present study is exceptional, and one has to keep in mind that

the mineral that is present might deviate in composition from ideal svanbergite. However, a reasonable XRD–Rietveld fit was obtained using a svanbergite model, and the values fit well with the chemical data.

It remains challenging to obtain an accurate description of the kaolinite structure for use in Rietveld refinement because of the various types of possible structural disorder. Various attempts to describe the structure and structural disorder of kaolinites have been published by Ufer *et al.* (2015) and Sakharov *et al.* (2016). Additional information on the disorder of kaolintes was provided by, for example, Brindley *et al.* (1986), and, more recently, Kogure *et al.* (2005) and Mercier & Page (2008). This topic will not be discussed here further because it will be addressed in a follow-up study. Instead, the XRD traces of three samples of the two promising deposits (Fig. 8) were compared using widely accepted methods for the interpretation of kaolinite diffraction data.
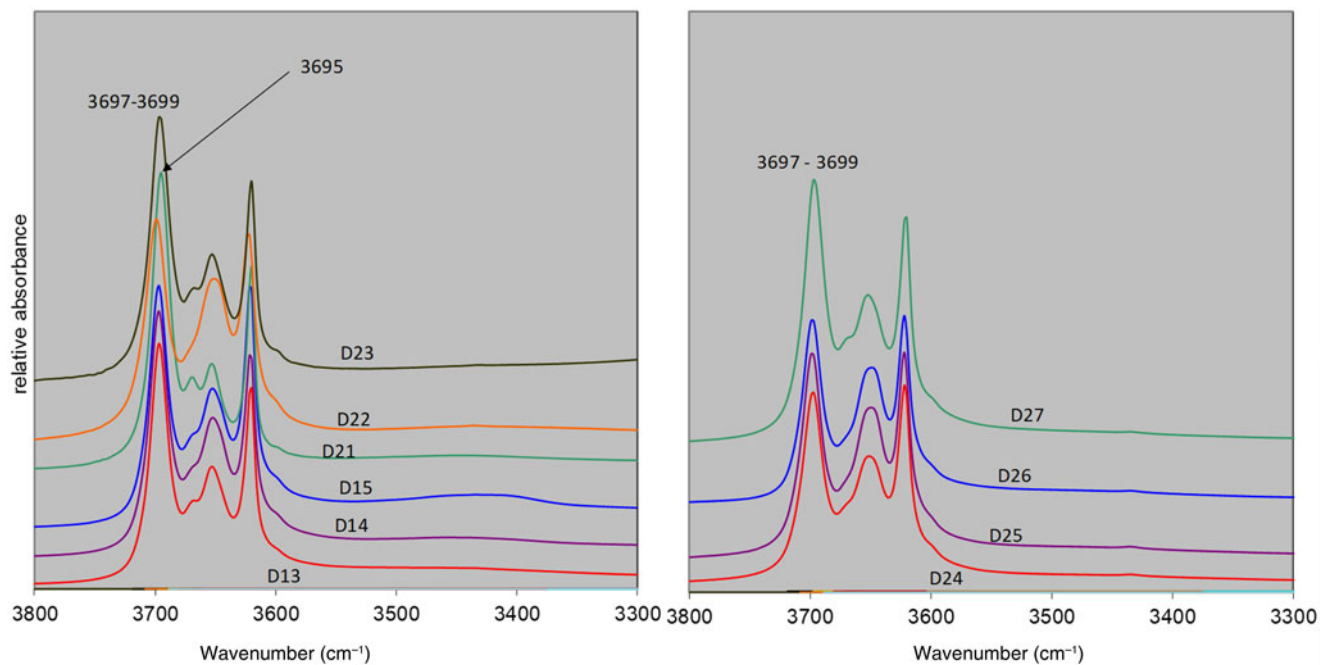
Fig. 9. FTIR spectra of the selected samples from the Kaédi (left) and Hassi Abyad (right) deposits.
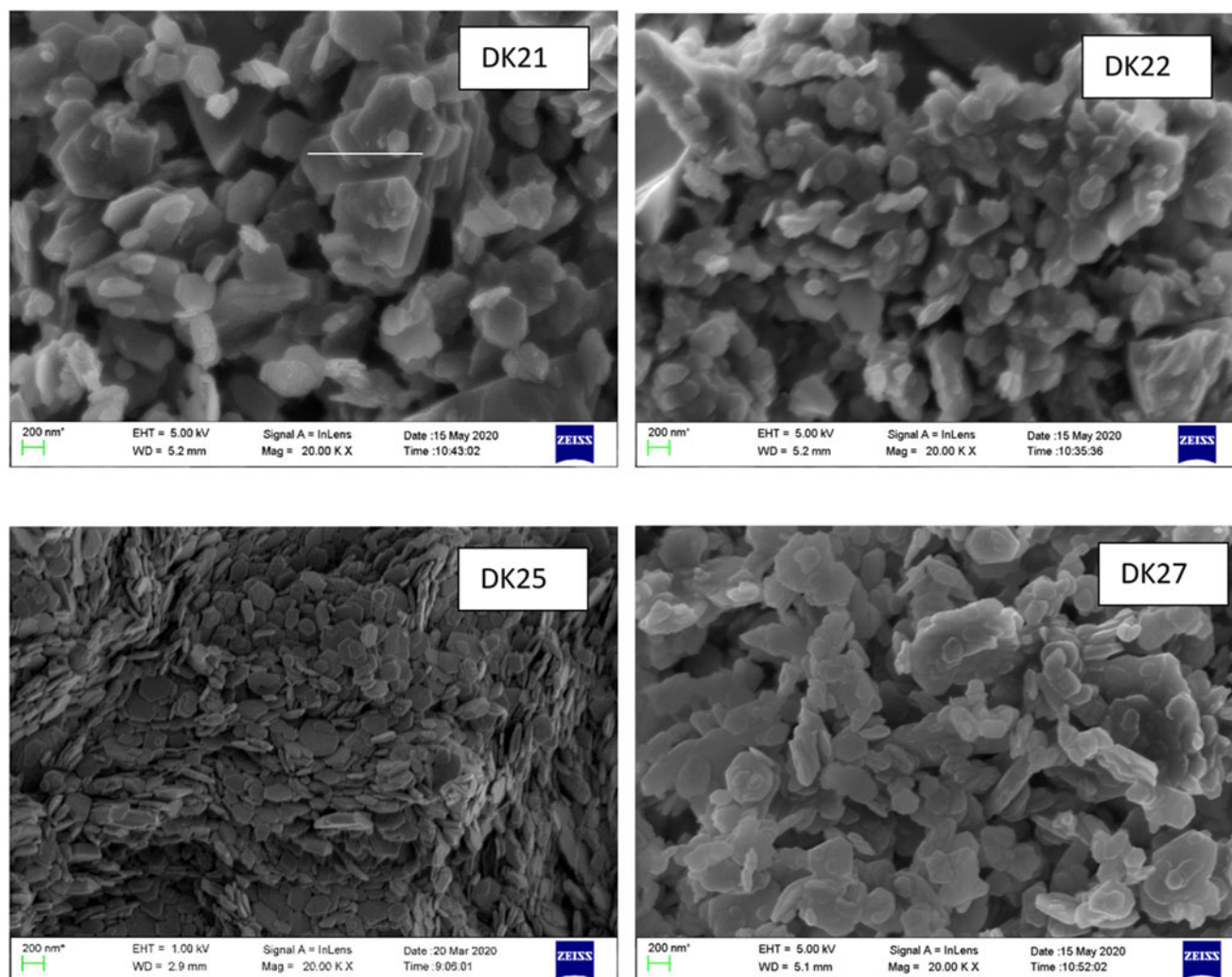
Fig. 10. SEM images of four samples selected because of their varying degrees of structural order in the sequence DK21 > DK 27 ≥ DK25 > DK22.

Table 5. Particle-size distribution of selected samples. The most significant size class is shown in bold.

Particle-size classes (µm)	DK13 Kaédi	DK14 Kaédi	DK15 Kaédi	DK21 Kaédi	DK22 Kaédi	DK23 Kaédi	DK24 Hassi Abyad	DK25 Hassi Abyad	DK26 Hassi Abyad	DK27 Hassi Abyad
				(mass%)					(mass%)	
<2	**75**	**61**	**71**	**54**	**26**	**62**	**72**	**90**	**88**	**88**
2.0–6.3	12	10	10	2	3	3	6	3	3	4
6.3–20	8	12	9	2	6	3	8	4	5	5
20–63	3	9	5	2	9	8	12	3	4	3
63–112	0	2	3	4	14	13	2	0	0	0
112–200	1	2	1	26	25	6	1	0	0	0
200–355	1	2	1	9	12	3	0	0	0	0
355–630	0	1	0	1	3	1	0	0	0	0
630–1120	0	0	0	0	1	0	0	0	0	0
1120–2000	0	1	0	0	0	0	0	0	0	0
>2000	0	0	0	0	0	0	0	0	0	0

Table 6. Results of ceramic tests of selected samples.

	DK13	DK14	DK15	DK21	DK22	DK23	DK24	DK25	DK26	DK27
Softening temperature (°C)	>1500	>1500	>1500	>1500	>1500	>1500	>1500	n.d.	n.d.	n.d.
Flowing temperature (°C)	>1500	>1500	>1500	>1500	>1500	>1500	>1500	n.d.	n.d.	n.d.
Shrinkage (%)										
1000°C	2.8	2.0	3.0	0.4	−0.5	1.0	2.9	5.3	5.3	4.4
1100°C	3.3	3.4	5.7	0.5	−0.3	1.7	3.9	6.0	6.2	5.2
1200°C	7.1	5.5	7.2	1.0	−0.3	2.9	5.3	12.8	13.4	12.2
1300°C	8.5	5.9	8.0	1.3	−0.4	3.0	4.8	16.4	17.0	15.1
Water uptake (%)										
1000°C	20.0	18.8	18.8	18.4	12.6	18.4	27.3	22.2	21.9	24.2
1100°C	19.2	16.4	13.4	18.5	12.4	17.5	25.2	24.0	20.6	22.7
1200°C	12.4	12.0	10.2	17.5	12.2	15.4	21.2	9.9	8.6	10.4
1300°C	8.9	10.7	8.7	16.3	12.2	14.8	21.6	3.8	3.0	4.9
Tensile strength (MPa)										
1100°C	1.4	1.8	3.1	0.3	0.7	0.8	1.3	0.8	1.1	1.1
1200°C	2.8	2.0	3.8	0.4	0.8	1.2	1.5	1.6	2.0	2.4
1300°C	3.4	2.7	4.5	0.5	0.9	1.5	2.2	2.5	3.2	3.5

Kaolinites from the two deposits showed significantly different diffraction traces. The green trace (Fig. 8) representing sample DK22 is dominated by quartz, and the d_{001} intensity of kaolinite is low because of the small kaolinite content of this sample. The d_{001} reflection of the remaining samples is sharp, but significant differences were found in the 2θ regions between 23–28° and 40–47°. The peaks between 40° and 47° might indicate a more dickitic character of the Hassi Abyad samples (stacking sequences with alternating octahedral vacancies) and a more kaolinitic character of the Kaédi samples (stacking sequences with equal octahedral vacancies). Sample DK22 would also be considered as showing dickitic character, but the kaolinite content is small, which results in lower intensities and thus increasing uncertainty. If present, the dickitic character might be interpreted as a type of disorder caused by a mix of dickitic and kaolinitic layer stacking. However, more work is necessary to verify the presence of dickitic stacking sequences in the Hassi Abyad samples. Additional *b*-axis disorder may exist, but this is also difficult to verify. Overall, the samples from Hassi Abyad showed a lesser degree of structural order compared to the samples from Kaédi.

Careful inspection of the XRD traces (7 h long-term measurements) showed no hints of mica or feldspars. This finding is supported by the chemical composition. The only layer silicate present is kaolinite. Therefore, only randomly orientated specimens were prepared.

IR spectroscopy

Selected samples were investigated by FTIR spectroscopy. The FTIR spectra are shown in Fig. 9.

FTIR spectroscopy may also be used to investigate the degree of structural order of kaolin minerals (Russell & Fraser, 1994; Awad *et al.*, 2018). Figure 9 shows the OH-stretching region of the IR spectra of the selected samples from the Kaédi and Hassi Abyad deposits. The 3670 cm^{-1} band intensity (v_2 in case of kaolinites) can be used to determine the so-called 'b-axis' disorder, a term often used to describe the IR spectra of kaolinite (Brindley *et al.*, 1986). The discussion about the exact meaning of this parameter, however, is not the subject of the present study; it is simply used as a proxy to characterize the various materials. Significant variability of the 3670 cm^{-1} band intensity (*b*-axis disorder) of samples from Kaédi was observed (Fig. 9, left). Most samples showed a pronounced shoulder at 3670 cm^{-1}, and sample DK21 showed a well-resolved band. Accordingly, the kaolinite from sample DK21 showed the least significant *b*-axis disorder and the kaolinite from sample DK22 showed the most significant *b*-axis disorder. The sample from Hassi Abyad, on the other hand,
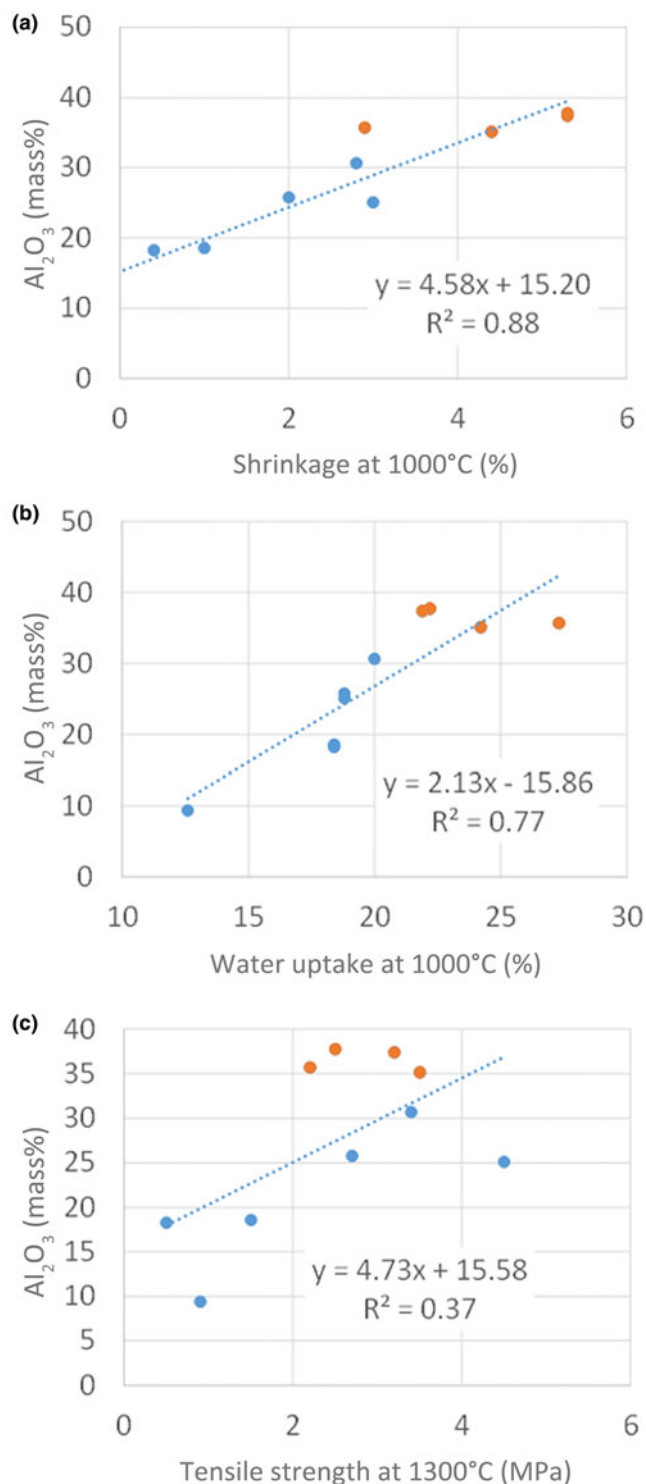
Fig. 11. Correlations of ceramic parameters with the Al₂O₃ contents of selected samples. (a) Shrinkage compared with Al₂O₃ content; (b) water uptake compared with Al₂O₃ content; (c) tensile strength compared with Al₂O₃ content.

been discussed by Brindley & Brown (1980), for example. The band positions of all of the samples varied from 3697 to 3699 cm^{-1}, corresponding to a Hinkley index of 0.2–0.4, indicating moderately disordered kaolinites. Only sample D21, which also showed the most intensive 3670 cm^{-1} band, pointing towards the least *b*-axis disorder, showed a v_1 band position of 3695 cm^{-1}, corresponding to a Hinkley index of 0.7 (based on Brindley *et al.*, 1986) and indicating a greater degree of structural order. A further possibility for characterizing the degree of structural order of kaolinites based on IR spectroscopy was published by Parker (1969). He considered the ratio of the v_1 (3700 cm^{-1}) and the v_4 (3625 cm^{-1}) bands, which reflects the ratio of OH groups at the outer particle surfaces and OH groups inside the particles. For samples DK24 to DK26, a v_1:v_4 ratio of ~1 was calculated. In the case of the Kaédi samples, on the other hand, a slightly more intense v_1 was observed.

SEM investigation

Four different samples selected based on their varying degree of structural order (as indicated by IR spectrometry) were investigated using SEM. The largest degree of structural order was found for sample DK21, followed by samples DK27 and DK25 (more or less similar), and the lowest degree of structural order was found for sample DK22. Representative SEM images of these four samples are shown in Fig. 10.

The largest kaolinite crystallites occur in sample DK21, which showed the greatest degree of structural order. The largest crystallites were ~1 µm and the particle size ranged between 0.2 and 1.0 µm (scale bar in Fig. 10). Both hexagonal and pseudohexagonal platy particles were observed. Kaolinite particles from sample DK22 with the least degree of structural order showed diameters of ~0.2 µm. Kaolinite particles of sample DK25 were slightly larger (0.2–0.4 µm). Sample DK27 showed kaolinite particle sizes ranging from 0.2 to 0.6 µm. All of the samples showed kaolinite particles with comparably high aspect ratios and (pseudo)hexagonal shapes, but of different diameters, which corresponded to the degree of structural order. The typical 'booklet' appearance of kaolinites was not observed. The morphology of kaolinites was discussed comprehensively by Fiore *et al.* (1995) and Zhang *et al.* (2017).

Particle-size distribution

The particle sizes of the selected samples are summarized in Table 5 (compare with Table 2).

The material from Hassi Abyad consists mainly of fine particles rarely exceeding 63 µm in size. As was expected, the dominant particle size class was the <2 µm fraction. The <2 µm content of the samples from this deposit ranged from 70 to 90 mass%. The greater values were observed for the kaolinite-rich materials. The samples from the Kaédi deposit might be classified into two groups based on the particle size. Samples DK13 to DK15 contained only 2–5 mass% <63 µm and up to 70 mass% <2 µm, but the remaining samples (DK21 to DK23) contained 20–30 mass% >63 µm and had considerably fewer particles of the <2 µm fraction. This result is in accord with the larger quartz content determined by XRD (Table 4).

Ceramic testing

Ten samples of the Hassi Abyad and the Kaédi deposits were selected for the testing of ceramic properties. The results are

did not display such variations, but instead showed a high degree of *b*-axis disorder (low intensity of the 3670 cm^{-1} band). Alternatively, the position of the v_1 stretching vibration of kaolinites can be used to estimate the Hinkley index, which has often been used to characterize the degree of structural disorder of kaolinites using XRD (Brindley *et al.*, 1986). Additional indices have
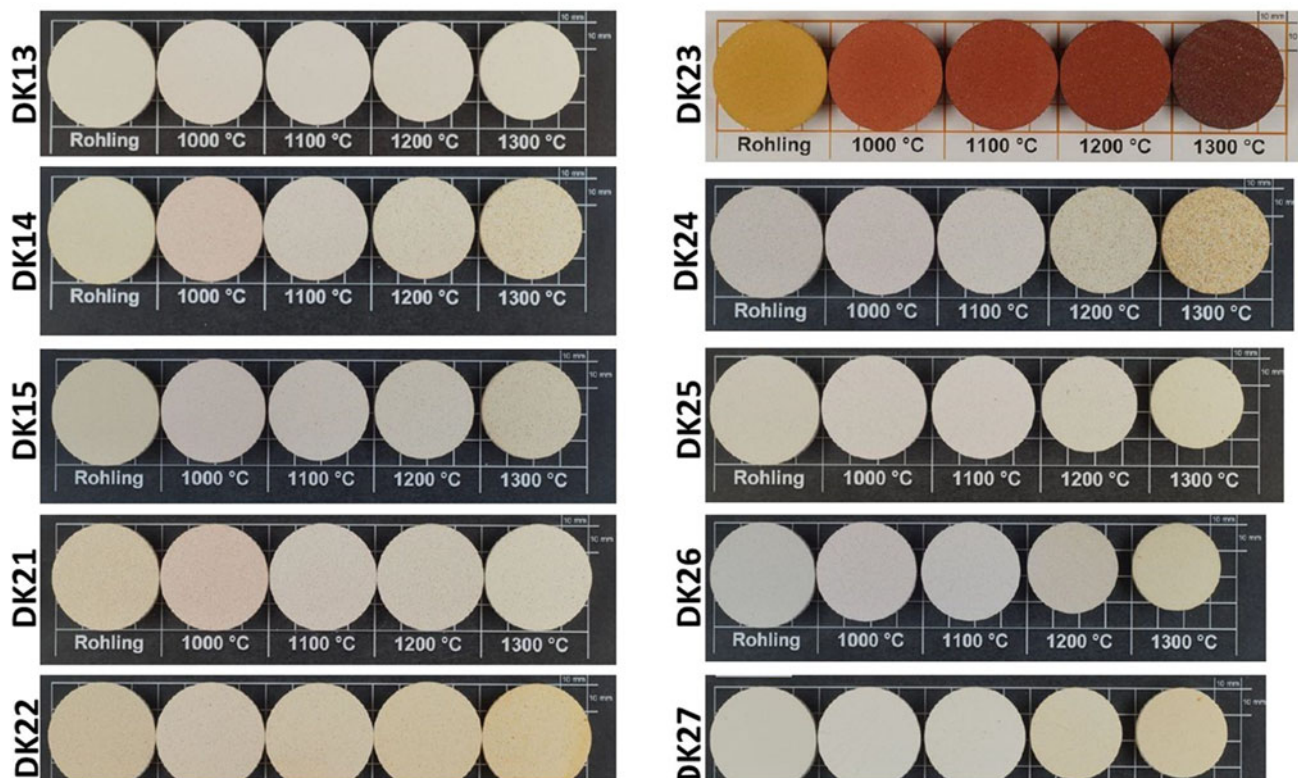
Fig. 12. Photographs of selected samples fired at various temperatures.

summarized in Table 6. In addition, the results were compared with the Al_2O_3 content, which largely reflects the kaolinite content.

The softening and flowing temperatures of all of the samples exceeded 1500°C (not determined for DK25 to DK27 because of their high Al_2O_3 contents). Therefore, these parameters could not be used to determine the ceramic properties of the samples.

A good correlation was observed between Al_2O_3 and shrinkage (Fig. 11a). A greater shrinkage was observed for samples with greater Al_2O_3 contents. A good correlation was observed for all temperatures. Sample DK22 did not show any shrinkage, probably because of the rather small kaolinite and large quartz contents. Sample DK24 showed a unique behaviour: a decrease in volume was observed between 1200°C and 1300°C, which was not observed for the other samples. This might be attributed to the calcite content because this is the only carbonate-bearing sample. This possible explanation, however, remains speculative.

The water-adsorption capacity (Fig. 11b), which can be used to determine the level of open porosity, is known to be related to the shrinkage. Samples with a large kaolinite content show a significant decrease in water uptake. As for the shrinkage case, sample DK22 did not follow this trend because of its small kaolinite content. In addition, sample DK24 did not show any significant change in its water-adsorption capacity at >1200°C, in contrast to the other samples. No explanation is currently offered for this unique behaviour. The regression coefficient of the water absorption–Al_2O_3 content correlation decreases with increasing temperature. At >1200°C, no trend is observed between the two parameters.

The tensile strength shows the weakest correlation with the Al_2O_3 content, which indicates that other parameters have to be considered. Samples DK13 to DK15 show similar tensile strengths, being the samples with the largest kaolinite contents (Fig. 11c). This might be explained by the microstructure after

firing, which includes the intergrowth of mullite and quartz (and other minor components).

The firing colour of kaolins is important for some ceramic applications. Photographs of samples after firing at various temperatures are shown in Fig. 12. The red colour of sample DK23 is attributed to its high Fe_2O_3 content. The brightest colours were observed for the samples of the Kaédi deposit. The samples from Hassi Abyad turned darker after firing at 1200°C; this was not observed for the samples from Kaédi. Both deposits, however, contain raw materials with bright colours, and they might be used for sanitary ware. All of the raw materials might be used for the production of ceramics. The samples with a large Al_2O_3 content from Hassi Abyad may be suitable for the production of refractory materials. The bright-firing samples might be used for sanitary ware, tableware or as technical ceramics. The materials with greater Fe_2O_3 contents, such as sample DK23, are potentially suitable for the production of bricks and/or roof tiles. Selective mining considering the various quality-determining parameters would provide the possibility of producing a range of different ceramic products for a wide range of applications.

Conclusions

Kaolin occurrences from three different regions in southern Mauritania were investigated. The kaolins show variable Al_2O_3 contents between 9% and 38%, which correspond to kaolinite contents of 23–96%. Kaolinite contents are greatest at Hassi Abyad and in some of the occurrences from the Kaédi region (>25% Al_2O_3 or >63% kaolinite). Materials from the Néma region contained less kaolinite (<50 mass%). As this region is also more difficult to access, the mineralogical investigations focused on the kaolins from the occurrences of the Kaédi and Hassi Abyad regions.

The degree of structural order of the kaolinites was assessed using both XRD and IR spectroscopy. Both methods proved a generally greater degree of structural order of the samples from the Kaédi deposit, but also greater variability of kaolinites from this deposit. The samples from Hassi Abyad were all similar but generally showed a lower degree of structural disorder.

All of the raw materials could be used for the production of ceramics. Other possible applications (e.g. filler, refractories, glass, etc.) were not tested. However, based on the comparably high purity, particularly of the samples from Hassi Abyad, the materials may be suitable for other applications as well. For example, the samples with large Al_2O_3 contents from Hassi Abyad might be suitable for the production of refractory materials. The samples with bright firing colours might be used for fine ceramics such as sanitary ware, tableware or as technical ceramics. The materials with greater Fe_2O_3 contents, such as sample DK23, may be suitable for the selective production of bricks and/or roof tiles. Selective mining considering the various quality-determining parameters would provide the possibility of producing a range of different ceramic products for a range of applications.

Future work will be devoted to the systematic exploration of the deposit based on drilling, XRD and XRF investigations of >1000 samples. The results will allow for a preliminary feasibility study, including the possible use of blending beds and/or selective mining. Due to the large kaolinite content in some layers, the material might also be interesting as a reference clay for scientific purposes.

References

Awad M.E., Amer R., López-Galindo A., El-Rahmanya M.M., García del Morale L.F. & Viseras C. (2018) Hyperspectral remote sensing for mapping and detection of Egyptian kaolin quality. *Applied Clay Science*, **160**, 249–262.

Baudet G., Baron M. & Hergibo P.L. (1987) *Étude préliminaire de la valoristion d'un échantillon de kaolin de Mauritanie*. Unpublished report, BRGM, Orléans, France, 85 pp.

Bergmann J., Friedel P. & Kleeberg R. (1998) BGMN – a new fundamental parameters based Rietveld program for laboratory X-ray sources, its use in quantitative analysis and structure investigations. *CPD Newsletter*, **20**, 5–8.

Brindley G.W. & Brown G. (eds) (1980) *Crystal Structures of Clay Minerals and Their X-Ray Identification*. The Mineralogical Society of Great Britain & Ireland, London, UK, 495 pp.

Brindley G.W., Kao C.C., Harrison J.L., Lipsicas M. & Raythatha R. (1986) Relation between structural disorder and other characteristics of kaolinites and dickites. *Clays and Clay Minerals*, **34**, 239–249.

de Jongh W.K. (1973) X-ray fluorescence analysis applying theoretical matrix correction. Stainless steel. *X-Ray Spectrometry*, **2**, 151–158.

Dewi R., Agusnar H., Alfian Z. & Tamrin (2018) Characterization of technical kaolin using XRF, SEM, XRD, FTIR and its potentials as industrial raw materials. *Journal of Physics: Conference Series*, **1116**, 042010.

Dill H.G. (2001) The geology of aluminium phosphates and sulphates of the alunite supergoup: a review. *Earth Science Reviews*, **53**, 35–93.

Dill H.G. (2016) Kaolin: soil, rock and ore. From the mineral to the magmatic, sedimentary, and metamorphic environments. *Earth Sciences Reviews*, **161**, 16–129.

DIN 51730 (2007) *Prüfung fester Brennstoffe – Bestimmung des Asche-Schmelzverhaltens (English: Testing of Solid Fuels – Determination of Fusibility of Fuel Ash)*. Beuth Verlag, Berlin, Germany, 19 pp.

DIN EN 993-1 (2019) *Methods of Test for Dense Shaped Refractory Products – Part 1: Determination of Bulk Density, Apparent Porosity and True Porosity; German version EN 993-1:2018*. Beuth Verlag, Berlin, Germany, 27 pp.

Döbelin N. & Kleeberg R. (2015) Profex: a graphical user interface for the Rietveld refinement program BGMN. *Journal of Applied Crystallography*, **48**, 1573–1580.

Ekosse G.-I.E. (2010) Kaolin deposits and occurrences in Africa: geology, mineralogy and utilization. Eastern Cape 5117, South Africa. *Applied Clay Science*, **50**, 212–236.

Fiore S., Huertas J., Huertas F. & Linares J. (1995) Morphology of kaolinite crystals synthesized under hydrothermal conditions. *Clays and Clay Minerals*, **43**, 353–360.

Harben P.W. (1992) *The Industrial Minerals Handybook. A Guide to Markets, Specification and Prices*. Metal Bulletin PLC, London, UK, 412 pp.

Harvey C.C. & Murray H.H. (1997) Industrial clays in the 21st century: a perspective of exploration, technology and utilization. *Applied Clay Science*, **11**, 285–310.

Hurst V.L. & Pickering S.M. Jr (1997) Origin and classification of Coastal Plain kaolins, southeastern USA, and the role of groundwater and microbial action. *Clays and Clay Minerals*, **45**, 274–285.

Kaufhold S. & Dohrmann R. (2013) The variable charge of dioctahedral clay minerals. *Journal of Colloid and Interface Science*, **390**, 225–233.

Kogel J.E. (2014) Mining and processing kaolin. *Elements*, **10**, 189–193.

Kogure T., Inoue A. & Beaufort D.F. (2005) Polytype and morphology analyses of kaolin minerals by electron back-scattered diffraction. *Clays and Clay Minerals*, **53**, 201–210.

Langer W.H. & Horton J.D. (2012) *Occurences des minérales rapporté de l'industrie et zones 'permissive' pour autres occurences dans la Mauritanie*. US Geological Survey, Reston, VA, USA, 22 pp.

Limam E., Ba O., Mohamed A.M. & Kuester D. (2017) *Rapport de Mission de Reconnaissance sur l'Évaluation des Ressources Exploitables de Calcaire et de Kaolin*. Unpublished report. OMRG, Nouakchott, Mauritania, 12 pp.

Limam E., Ba O. & Mohamed A.M. (2018) *Rapport de Mission de Reconnaissance des Kaolins du Dhar (Axe Néma – Oualata)*. Unpublished report. OMRG, Nouakchott, Mauritania, 18 pp.

Meier L.P. & Kahr G. (1999) Determination of the cation exchange capacity (CEC) of clay minerals using the complexes of copper (II) ion with triethylenetetramine and tretraethylenepentamine. *Clays and Clay Minerals*, **47**, 386–388.

Mercier P.H.J. & Page Y.L. (2008) Kaolin polytypes revisited *ab initio*. *Acta Crystallographica. Section B, Structural Science*, **64**, 131–143.

Murray H. (1998) Kaolin minerals: their genesis and occurrences. Pp. 67–89 in: *Hydrous Phyllosilicates (Exclusive of Micas)* (S.W. Bailey, editor). Mineralogical Society of America, Washington, DC, USA.

Njoya A., Nkoumbou C., Grosbois C., Njopwouo D., Njoya D., Courtin-Nomade A. *et al.* (2006) Genesis of Mayouom kaolin deposit (western Cameroon). *Applied Clay Science*, **32**, 125–140.

OMRG (2015) Office Mauritanien de Recherches Géologiques. Géologie générale de la Mauritanie. Available from https://anarpam.mr/activites-geologiques/#

Parker T.W. (1969) A classification of kaolinites by infrared spectroscopy. *Clay Minerals*, **8**, 135–141.

Pitfield P.E.J., Key R.M., Waters C.N., Hawkins M.P.H., Schofield D.I., Loughlin S. & Barnes R.P. (2004) *Notice explicative des cartes géologiques et gîtologiques à 1/200 000 et 1/500 000 du Sud de la Mauritanie. Volume 1 – Géologie*. DMG, Ministère des Mines et de l'Industrie, Nouakchott, Mauritania, 547 pp.

Russell J.D. & Fraser A.R. (1994) Infrared methods. Pp. 11–67 in: *Clay Mineralogy: Spectroscopic and Chemical Determinative Methods* (M.J. Wilson, editor). Chapman and Hall, London, UK.

Sakharov B.A., Drits V.A., McCarty D.K. & Walker G.M. (2016) Modeling powder X-ray diffraction patterns of the clay minerals society kaolinite standards: KGA-1, KGA-1b, AND KGa-2. *Clays and Clay Minerals*, **64**, 314–333.

Ufer K., Kleeberg R. & Monecke T. (2015) Quantification of stacking disordered Si–Al layer silicates by the Rietveld method: application to exploration for high-sulphidation epithermal gold deposits. *Powder Diffraction*, **30**, 111–118.

Zhang S., Liu Q., Yang Y., Wang D., He J. & Sun L. (2017) Preparation, morphology, and structure of kaolinites with various aspect ratios. *Applied Clay Science*, **147**, 117–122.